A consumer-facing application for radiance field-based 3D reconstruction enables accessible measurement of urban tree structure

Sruthi M. Krishna Moorthy[1,2,3], Maren Lechner[2], Henry Cerbone[2], Bhavya Palgudi[2], Jake Dudderidge[2], Graham Taylor[2], Roberto Salguero-Gómez[1,2]

[1]Pembroke College, University of Oxford, Oxford, United Kingdom

[2]Department of Biology, University of Oxford, Oxford, United Kingdom

[3]Environmental Change Institute, University of Oxford, Oxford, United Kingdom

[*]**Corresponding author**: Department of Biology, Life and Mind Building, S Parks Rd, Oxford OX1 3EL

sruthi.krishnamoorthyparvathi@pmb.ox.ac.uk

Abstract

Urban forests are key in mitigating the effects of climate change and urbanisation on human well-being. Yet, evaluating and managing these benefits requires accurate, scalable monitoring of trees. Laser scanners operated from ground-based and airborne platforms have enabled urban trees to be monitored in unprecedented structural detail and across large spatial extents, respectively. However, important trade-offs remain among cost, spatial coverage and the level of structural detail captured. Recent advances in radiance-field-based continuous 3D reconstruction offer a more accessible alternative, while their integration into consumer-facing smartphone applications has opened new opportunities for participatory monitoring via citizen science. However, these approaches remain insufficiently validated for urban trees. We evaluated radiance-field-based 3D tree reconstructions generated from smartphone videos using the consumer-facing Luma AI platform, comparing them with terrestrial laser scanning (TLS) reference data across leaf-on and leaf-off seasons and a gradient of surrounding vegetation complexity. Seventy-eight trees across fourteen urban plots of size 20 m by 20 m were surveyed under leaf-on and leaf-off conditions. Luma AI produced usable reconstructions for 63 trees in summer and 66 in winter, with no significant seasonal difference in failure rate (19.2% versus 15.4%; McNemar $p = 0.629$). Tree height showed strong agreement with TLS in both summer and winter (CCC = 0.887 and 0.866, respectively), while crown-area agreement was lower, particularly during winter (CCC = 0.795 and 0.643). Fine branches, which were occluded in summer but exposed during winter data collection, were more difficult to reconstruct, resulting in winter trees having higher precision but lower recall

and overall lower reconstruction fidelity than summer trees (F1 = 0.366 ± 0.220 versus 0.420 ± 0.232). Nevertheless, this loss of geometric completeness did not prevent the extraction of useful whole-tree structural metrics. Reconstruction fidelity declined with increasing tree density and total crown area during summer (Spearman's ρ = −0.677 and −0.692), when foliage increased occlusion. Consumer-facing applications enabling continuous-scene reconstruction methods therefore offer considerable potential for large-scale participatory monitoring of trees in open urban landscapes and could help democratise structural monitoring in other sparsely wooded ecosystems.

Keywords: Citizen science, Gaussian splatting, Image-based 3D reconstruction, LiDAR, NeRF, Tree monitoring, Urban forestry.

1. Introduction

Urbanisation is a defining feature of contemporary human demographic growth, with more than half of the global population now living in urban areas (United Nations Department for Economic and Social Affairs 2020). Furthermore, the extent of urbanisation is expected to increase substantially over the coming decades (Seto et al. 2012). Under different climate and socioeconomic scenarios, the global urban land area is projected to expand by approximately 40–67% by 2030 compared to the past decade (Seto et al. 2012). However, both the proportion of people living in urban areas and the rate of urban expansion vary considerably among countries (X. Li et al. 2019). In the United Kingdom, for example, approximately 80% of the population lives within just 9% of the country's urban areas, with London substantially more populous than any other UK urban area (Williams 2009). Furthermore, the spatial extent of urban areas in the UK is projected to increase by 20% by 2050 (X. Li et al. 2019). As an increasing proportion of the world's population lives in cities (United Nations Department for Economic and Social Affairs 2020), understanding how urbanisation interacts with climate change to influence human health and well-being is becoming increasingly important (Das et al. 2024).

Increased urbanisation is associated with a range of environmental and societal challenges (Moore et al. 2003). These examples include elevated temperatures caused by the urban heat-island effect (Parker 2010), air pollution (Sicard et al. 2023), increased flood risk (Feng et al. 2021), loss of biodiversity (Hald-Mortensen 2023), and reduced opportunities for interaction with nature (Gaston and Soga 2020). Urban green spaces, including parks, gardens, and street trees, are increasingly recognised as an important

nature-based approach for mitigating some of these adverse effects (F. Zhang and Qian 2024). Vegetation can provide cooling through shading and evapotranspiration (Taylor et al. 2024; Daelman et al. 2026), minimize flood risk (Dong et al. 2025), and contribute to carbon storage and sequestration (Nowak and Crane 2002). At the same time, urban green spaces provide habitat and resources for a wide range of species and can enhance local biodiversity (Threlfall et al. 2017; Aronson et al. 2017). Their benefits also extend directly to people: access to parks and other green spaces has been associated with improved mental well-being, opportunities for recreation and physical activity, and greater social interaction (F. Zhang and Qian 2024; Bertram and Rehdanz 2015; Douglas et al. 2017). Urban trees are particularly important components of these green spaces because their three-dimensional structure and longevity allow them to deliver many of these climatic, ecological and societal benefits simultaneously (Daelman et al. 2026; Seamans 2013).

Quantifying the contributions of urban trees to climate regulation, biodiversity and human well-being requires methods that can characterise tree structure accurately and at scale. Tree size and architecture support estimates of biomass and carbon stocks (Wilkes et al. 2018; Davenport et al. 2026), modelling of shading and evaporative cooling (Daelman et al. 2026), and assessments of tree condition, management and future planting needs (Drénou et al. 2015; Pretzsch et al. 2023). Although attributes such as diameter at breast height and tree height are conventionally measured using diameter tapes and rangefinders, laser scanning can capture tree structure in substantially greater detail. Airborne laser scanning provides broad spatial coverage, whereas terrestrial and mobile laser scanning produce high-resolution representations of individual trees(D’hont

et al. 2024). However, airborne observations may omit smaller trees and struggle to delineate overlapping crowns(Lindberg and Holmgren 2017; Suárez et al. 2005), while terrestrial and mobile systems remain relatively expensive and require specialist equipment and processing (Calders et al. 2020; Maeda et al. 2025). While the emergence of lower-cost laser scanners is beginning to make terrestrial three-dimensional data acquisition more affordable (Mokroš et al. 2021; Výbošťok, Chudá, Tomčík, et al. 2025), consumer-device LiDAR and applications such as ForestScanner have made measurements such as DBH more accessible (Tatsumi et al. 2023; Howie and De Stefano 2024; Tsuzuki and Inoue 2026). However, their short operating range limits the capture of complete large-tree structure (Mokroš et al. 2021). The need for more accessible technology to monitor vegetation has increased interest in reconstructing three-dimensional tree structure from conventional imagery acquired using widely used cameras, including those present on modern smartphones (Roberts et al. 2019; Ghanbari Parmehr and Amati 2021; Výbošťok, Chudá, Skladan, et al. 2025).

Image-based reconstruction of vegetation structure has long been explored using Structure-from-Motion photogrammetry and Multi-View Stereo, which can derive tree attributes from overlapping photographs or video without dedicated ranging sensors (Miller et al. 2015; Z. Chen et al. 2025; Iglhaut et al. 2019). However, branching complexity, occlusion, repetitive textures and variable illumination remain challenging for conventional photogrammetry(Sadeghian et al. 2022; Iglhaut et al. 2019). Neural Radiance Fields (Mildenhall et al. 2020) and 3D Gaussian Splatting (Kerbl et al. 2023) have transformed image-based 3D reconstruction by representing scene appearance continuously, enabling photorealistic rendering from previously unseen viewpoints

(Giaquinto et al. 2026; Y. Zhang et al. 2026; Muñoz-Bañón et al. 2026; Arshad et al. 2024). Furthermore, consumer applications such as Luma AI make these techniques accessible using smartphone videos and limited technical expertise(Cerbone et al. 2025; Rangelov et al. 2024). This accessibility could support citizen science by enabling participants to contribute systematically acquired imagery rather than manually measured tree attributes(Tsuzuki and Inoue 2026; Woo et al. 2024; Wheeler et al. 2025). Structural measurements could then be extracted through a consistent analytical workflow, expanding opportunities for detailed and scalable urban-tree monitoring.

Despite the increasing accessibility of image-based three-dimensional reconstruction, it remains unclear whether models generated using consumer-facing applications can reproduce tree structure with sufficient accuracy for quantitative urban-vegetation monitoring. Here, we evaluate Luma AI (*Luma* 2026), a freely accessible smartphone application that enables three-dimensional scene reconstruction from video without requiring dedicated ranging sensors or specialist reconstruction software. We use Luma AI as a representative example of an emerging class of consumer-facing AI-based 3D reconstruction tools, for which the combination of readily available hardware, guided data acquisition and automated reconstruction could substantially reduce barriers to large-scale and participatory data collection. We compare tree models generated from smartphone imagery with high-resolution terrestrial laser scanning (TLS) as a reference representation of three-dimensional tree structure. Using trees in the University Parks in Oxford, UK, surveyed under both summer (leaf-on) and winter (leaf-off) conditions, we assess the ability of the smartphone-derived reconstructions to recover tree height and crown structure and examine how reconstruction performance varies with season.

2. Methods

2.1. Study site

This study took place at the University Parks, Oxford, United Kingdom (approximately 51.76° N, 1.25° W). The University Parks form a managed urban greenspace situated between central Oxford and the River Cherwell. The site comprises a diverse collection of rare and historic tree species. The park is a Grade II listed landscape within the Oxford Central Conservation Area and is locally designated as a site of ecological interest (University of Oxford, University Parks).

2.2. Sampling strategy

We designed our sampling approach to represent plots along a gradient of increasing vegetation density ranging from sparsely vegetated plots with isolated or widely spaced trees to plots containing closely spaced stems and overlapping crowns. To this end, we selected fourteen 20 m × 20 m plots distributed within the University Parks to capture variation in tree density and spacing, height composition, and canopy arrangement. Figure 1 shows the plot locations in relation to all the mapped trees within the park. We classified the plots according to the number of trees within their boundaries. Low-density plots contained fewer than four trees, medium-density plots contained four to six trees, and high-density plots contained more than six trees. Our study design comprised three low-density plots, seven medium-density plots and four high-density plots with the

individual plots containing anywhere between one and 15 trees. Overall, the dataset comprised 78 trees across the 14 plots with their heights ranging from 0.89 to 21.71 m.

2.3. Data collection

To evaluate how foliage and seasonal differences in canopy occlusion affected reconstruction performance, we collected both TLS and smartphone video data from the same fourteen plots during both leaf-on (summer) and leaf-off (winter) seasons. Summer data were collected between September and October 2025, and winter data were collected between January and February 2026. Data were collected on dry days under low-wind conditions, with smartphone videos recorded only when the focal tree exhibited little to no movement. TLS and smartphone video data were acquired during both campaigns to enable direct seasonal comparisons while controlling for plot location and tree identity.

2.3.1. Terrestrial laser scanning

We used TLS as the reference data because it provides high-resolution three-dimensional measurements of tree structure and has been extensively validated against manually measured structural attributes (D'hont et al. 2024; Terryn et al. 2024). We used a Leica RTC360 TLS (Leica Geosystems AG, Heerbrugg, Switzerland) in high-resolution mode and scanned each 20 m × 20 m plot from five scan positions with one near each of the four plot corners and one at the plot centre. Spherical control targets distributed within and around the plot provided common reference points for registering the five scans. Scan registration was performed in Leica Cyclone software, producing a single registered

plot-level TLS point cloud. The registered point clouds were subsequently exported in Polygon File Format (.ply) for further processing.

2.3.2. Smartphone video capture

To evaluate whether tree structure could be reconstructed using widely available, non-specialist consumer hardware, smartphone videos were collected for the same plots and trees using a Samsung Galaxy A56 5G smartphone (SM-A566B) running Android 15. A Samsung device was selected as 70% of the global smartphone users use Samsung, making the selected hardware relevant to a broad potential user base (Vanage 2025). We recorded videos using the native Samsung camera application with its default video settings, corresponding to a resolution of 1920 × 1080 pixels and a frame rate of 30 frames per second. No specialist capture application or manual camera configuration was used. Each video acquisition focused primarily on one tree. The operator moved around the focal tree to obtain overlapping views of its stem and crown from multiple directions. Consequently, the focal tree was generally reconstructed at the highest quality, whereas surrounding trees and peripheral vegetation received fewer overlapping views and were reconstructed at lower fidelity. The mean per-tree video-recording duration was 4.23 ± 1.89 min during summer and 4.54 ± 1.86 min during winter. Because reconstruction from RGB video alone does not recover absolute real-world scale, an object of known dimensions (a coloured 30 cm ruler and/or a calibration cube) was placed within each recorded scene to provide an external metric reference (Figure S1). The known dimensions of the reference object were subsequently used to scale the reconstructed point clouds to real-world dimensions (Figure S1). The videos were uploaded to the Luma

AI web platform (*Luma Is Your Creative Partner* 2026) and processed into three-dimensional reconstructions. The resulting point clouds in .ply format were downloaded directly from the platform for subsequent processing.

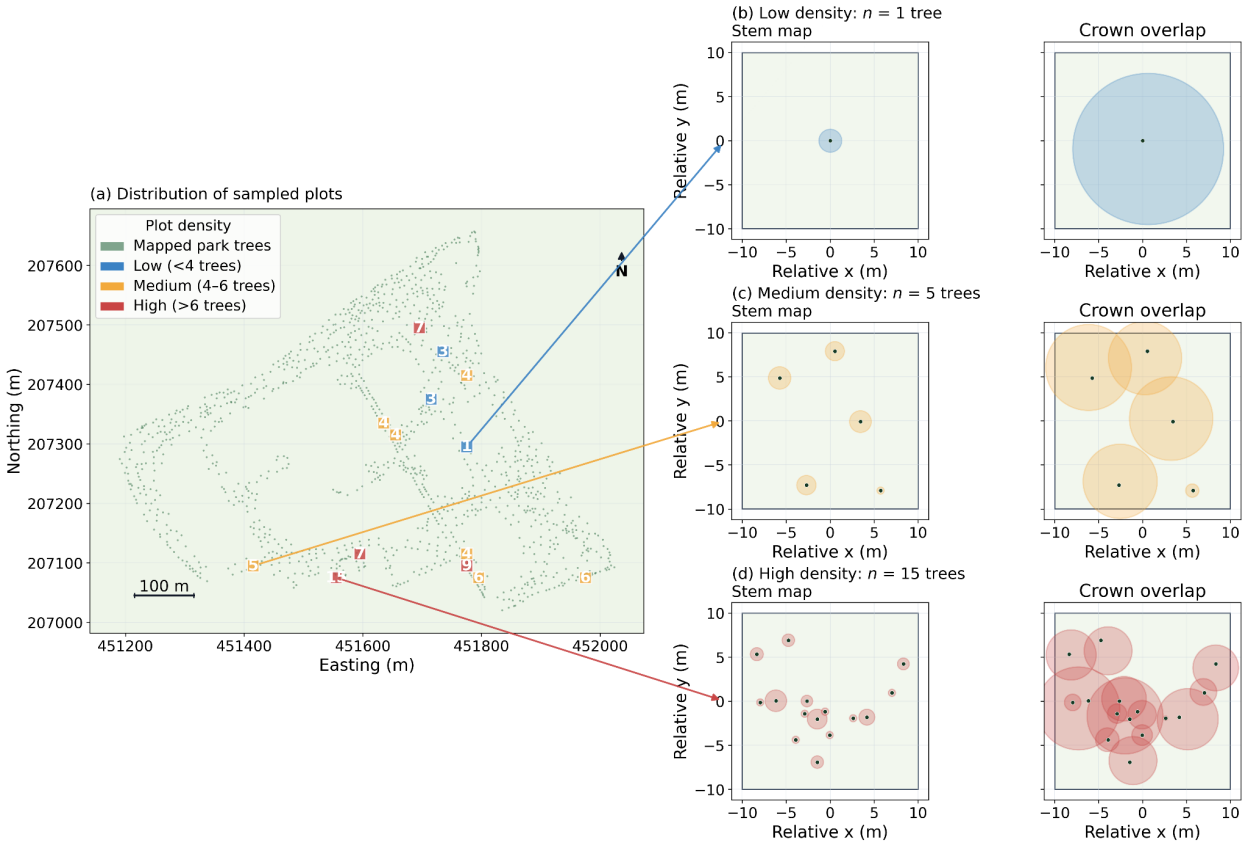


Figure 1: Distribution and spatial structure of the 14 sampled plots in University Parks, Oxford to evaluate smartphone-based tree reconstruction across different levels of surrounding vegetation density. (a) Locations of the 20 m × 20 m plots in relation to mapped park trees. Plot colours indicate tree-density class: low (<4 trees), medium (4–6 trees) or high (>6 trees). Panels (b–d) show representative low-, medium- and high-density plots, respectively. For each example, the stem map shows tree positions, while the crown map shows the spatial arrangement and potential overlap of TLS-derived crown footprints.

2.4. Data processing

To enable direct seasonal comparison, the winter TLS point cloud for each plot was co-registered to the corresponding summer point cloud in CloudCompare (version 2.13.2) (Girardeau-Montaut 2016). An initial manual alignment was performed by identifying at least three corresponding points that were clearly visible in both summer and winter point clouds. Following co-registration, the same 78 trees were manually isolated and cleaned from the summer and winter TLS point clouds to produce paired tree-level reference datasets. Each video submitted to the Luma AI platform produced a point cloud representing a single target tree. The resulting individual-tree point clouds were downloaded and manually cleaned in CloudCompare to remove points associated with the ground, neighbouring trees and other surrounding objects.

Two versions of each successfully reconstructed Luma AI point cloud for two seasons were subsequently produced. First, each cleaned Luma AI point cloud was scaled and transformed directly to its corresponding TLS-derived tree point cloud. This TLS-based scaling represented a best-case alignment scenario in which differences caused by scale were minimised, allowing the remaining disagreement between the point clouds to be attributed primarily to the radiance-field reconstruction and subsequent cleaning. The transformation also placed the Luma AI and TLS point clouds in a common coordinate system, enabling direct tree-level comparison.

Second, the Luma AI point clouds were scaled independently using the known dimensions of the coloured 30 cm ruler or calibration cube included in the recorded scene. Using CloudCompare, we manually segmented the scaling object from the point clouds,

calculated the scaling factor using the known dimensions and then scaled the whole tree point cloud (Figure S1). This approach represented the scaling procedure that could be applied without access to TLS reference data.

2.5. Structural metric extraction

We extracted two key structural metrics from the TLS and TLS-scaled Luma AI point clouds: height and crown area. Diameter at breast height (DBH) was not evaluated because many trees had irregular or multiple stems or stems branching from close to the base that would have required manual delineation of the trunk. The same metrics were also calculated from independently scaled Luma AI point clouds to assess the effect of independent scaling on the extracted metrics. Tree height was estimated from the vertical extent of each point cloud as the difference between the maximum and minimum extent of the z coordinate (Figure S2a). Crown area was estimated from the horizontal projection of the complete tree point cloud. The XY coordinates were spatially subsampled using a 0.05 m grid, and a two-dimensional convex hull was fitted around the resulting points. The crown area was calculated as the area enclosed by this convex hull (Figure S2b).

2.6. Evaluation metrics

Luma AI reconstruction success was first evaluated for all 78 target trees in each season. A reconstruction was considered successful when a usable individual-tree point cloud was available for metric extraction; otherwise, it was classified as failed. Seasonal failure rates were calculated as the number of failed reconstructions divided by the total number

of target trees. Because the same trees were surveyed during both seasons, the difference in reconstruction outcome between summer and winter was evaluated using an exact McNemar test for paired binary observations (Lachenbruch 2014).

The 3D reconstruction quality of the successfully generated and scaled Luma AI point clouds was evaluated using voxel-based metrics. Both TLS and TLS-scaled Luma AI point clouds were discretised onto a common three-dimensional grid with a voxel size of 10 cm. A 10 cm voxel size was used for evaluation to mitigate the impact of co-registration errors inherent in comparing point clouds of different resolutions. Sensitivity analysis of voxel sizes from 1 cm to 12.5 cm demonstrated that at smaller voxel sizes, these minor spatial offsets dominate the metric (Figure S3). Although the seasonal variation between summer and winter becomes consistent from the 5 cm resolution onward, the rapid increase in F1 scores indicates the metric is still highly sensitive to resolution at that scale. Beyond 10 cm, the F1 scores begin to stabilize, making it an appropriate threshold for the primary analysis. Overlapping occupied voxels were then used to calculate intersection over union (IoU), precision, recall and the F1 score (Cherlet et al. 2026). Precision represented the proportion of occupied Luma AI voxels that corresponded to occupied TLS voxels, whereas recall represented the proportion of occupied TLS voxels recovered by the Luma AI reconstruction. The F1 score was calculated as the harmonic mean of precision and recall, while IoU represented the ratio between the intersection and union of the two occupied voxel sets.

To assess agreement between TLS-scaled Luma AI and TLS-derived height and crown area, we used concordance- and error-based metrics. Specifically, agreement in height and crown area was assessed separately using Lin’s concordance correlation coefficient

(CCC) (Lin 1989). Signed percentage error was calculated to quantify the direction of disagreement, while absolute percentage error quantified its magnitude. Agreement between TLS and TLS-scaled Luma AI point clouds was evaluated separately for each season using all successful reconstructions available during that season. This analysis included 63 trees in summer and 66 trees in winter.

The influence of the scaling procedure was evaluated by comparing structural measurements derived from the independently scaled Luma AI point clouds with those derived from the corresponding TLS-scaled Luma AI point clouds. Independent scaling required the reference ruler or calibration cube to be reconstructed with sufficient fidelity for its dimensions to be identified. For some trees, a usable Luma AI reconstruction could be scaled and aligned directly to TLS, but an independent scale factor could not be derived because the reference object was absent, incompletely reconstructed or insufficiently distinct in the point cloud. These trees were retained for the principal TLS–Luma AI evaluation but excluded from the evaluation of independent scaling. The scaling comparison was therefore restricted to trees for which both independently scaled and TLS-scaled Luma AI point clouds were available, comprising 54 trees in summer and 64 trees in winter. Agreement in tree height and crown area between the two scaling approaches was quantified separately for each season using Lin's CCC. The TLS-based procedure represented a best-case scaling and alignment scenario, whereas independent scaling represented an approach that did not require access to TLS data. This analysis quantified the extent to which scaling influenced the structural measurements independently of the underlying Luma AI reconstruction.

2.7. Plot competition and reconstruction performance

Dense surrounding vegetation was expected to reduce Luma AI reconstruction performance because it made it more difficult to capture complete and unobstructed imagery of the target tree. Vegetation occlusion and increased scene complexity could also make it more difficult for the reconstruction pipeline to identify and match common visual features across successive video frames. The effect of surrounding vegetation on Luma AI performance was therefore evaluated using two plot-level indicators of competition. The first was tree density, represented by the number of trees within each 20 × 20 m^2 plot. Plots containing fewer than four trees were classified as low density, plots containing four to six trees as medium density and plots containing more than six trees as high density. The second indicator was total crown area, calculated as the sum of the TLS-derived crown areas of all trees within each plot. Tree count represented the number of potential neighbouring competitors, whereas total crown area represented the overall amount of canopy occupying the plot.

Competition was assessed in relation to Luma AI failure rate, voxel F1 score, absolute percentage height error and absolute percentage crown-area error. Except for reconstruction failure, which was evaluated for all target trees, these performance measures were calculated from the TLS-scaled Luma AI point clouds of successfully reconstructed trees. Tree-level F1 scores and absolute percentage errors were averaged within each plot before analysis. Associations between each plot-level performance measure and the two competition indicators, tree count and total TLS-derived crown area,

were evaluated separately for summer and winter using Spearman's rank correlation coefficient (ρ).

3. Results

3.1. Reconstruction success across seasons

Luma AI generated usable tree-level point clouds for 63 of the 78 target trees during summer and 66 of the 78 trees during winter. The corresponding reconstruction failure rates were 19.2% in summer (15/78; exact 95% CI: 11.2–29.7%) and 15.4% in winter (12/78; exact 95% CI: 8.2–25.3%; Figure 2). Five of the same trees failed to produce usable reconstructions in both seasons. The exact McNemar test found no evidence of a difference in reconstruction success between seasons ($p = 0.629$).

Reconstruction outcome was not significantly associated with the structure of the target trees. TLS-derived tree height did not differ between successfully and unsuccessfully reconstructed trees in either summer (Mann–Whitney U test, $p = 1.000$) or winter ($p = 0.210$; Figure S4). Similarly, TLS-derived crown area did not differ according to reconstruction outcome in summer ($p = 0.348$) or winter ($p = 0.863$; Figure S5). These results indicate that reconstruction failure was not clearly determined by the size of the target tree.

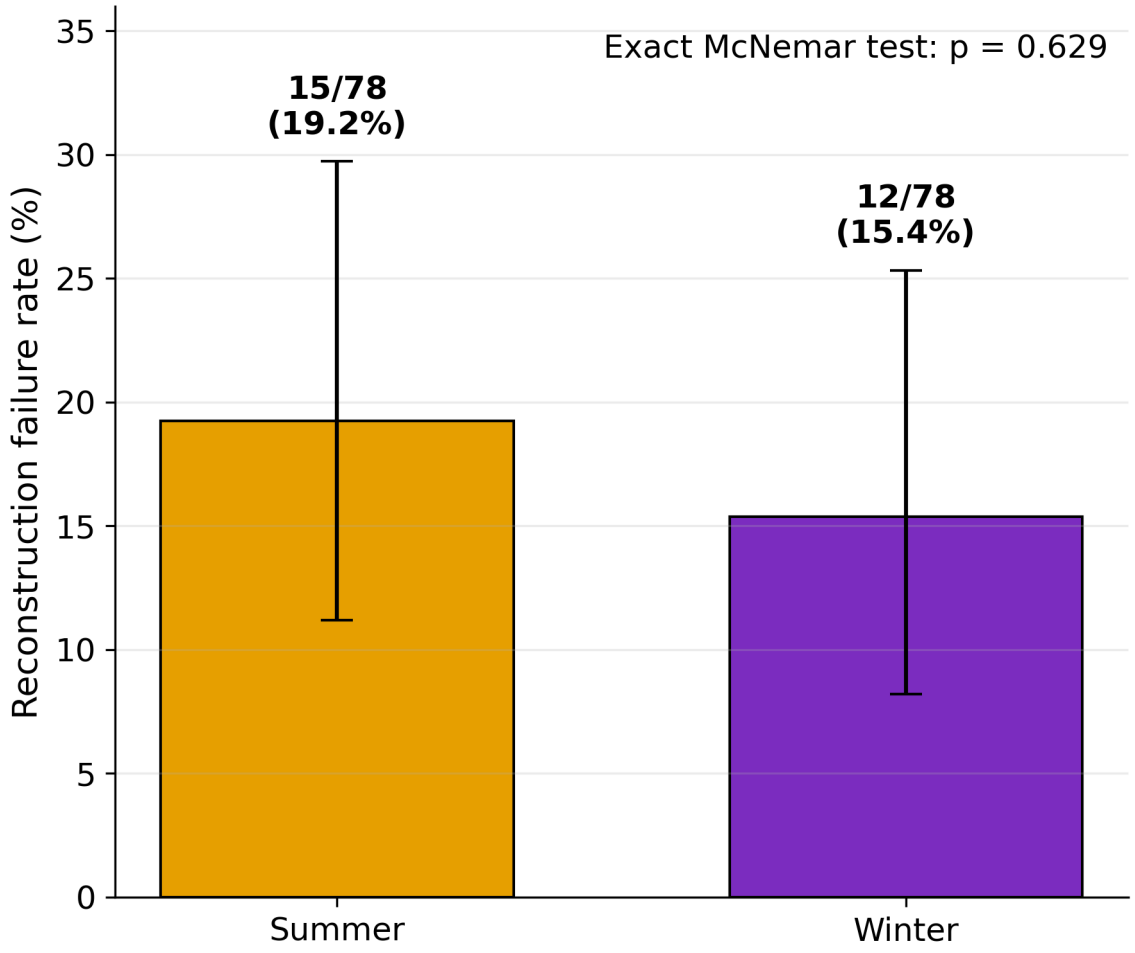


Figure 2: Luma AI reconstruction failure rates did not differ significantly between summer and winter. The reconstruction failure rates are shown for the same 78 target trees surveyed during summer and winter. The seasonal difference in the paired binary reconstruction outcomes was evaluated using an exact McNemar test.

3.2. Reconstruction quality of Luma AI point clouds

Voxel-based geometric agreement differed between seasons for the 56 trees successfully reconstructed in both summer and winter (Figure 3). Mean F1 was higher in summer (0.420 ± 0.232) than in winter (0.366 ± 0.220; paired Wilcoxon signed-rank test, p =

0.033). IoU showed the same seasonal pattern as F1 and was higher in summer (0.293 ± 0.194) than in winter (0.248 ± 0.184; $p = 0.051$). However, F1 score showed a clear negative trend with tree height in both summer (Spearman's $\rho = -0.733$, $p < 0.001$) and winter ($\rho = -0.616$, $p < 0.001$; Figure S6). Vertical distribution of the tree-level F1 score across all the plots further showed that voxel agreement was generally greatest near the tree base and declined towards the upper stem and crown (Figure S7). Smoothed plot-level vertical F1 profiles indicated that the height at which median F1 had declined by 20% varied among plots and seasons, demonstrating that the loss of geometric completeness was not associated with a single absolute height threshold. Across plots, median F1 declined by more than 20% at a height of 3.50 m during summer (IQR 3.00–4.38 m) and 2.25 m during winter (IQR 1.75–2.75 m). Instead, the decline depended on the tree height and local conditions within each plot.

While the overall F1 score was slightly lower, winter reconstructions had substantially higher precision (0.733 ± 0.210) than summer reconstructions (0.556 ± 0.187; $p < 0.001$), whereas recall was lower in winter (0.272 ± 0.203) than in summer (0.375 ± 0.238; $p < 0.001$). Thus, voxels present in the winter Luma AI reconstructions were more likely to correspond to the TLS reference, but winter reconstructions recovered a smaller proportion of the complete TLS-derived tree structure. This reduction in completeness outweighed the improvement in precision, resulting in lower overall F1 during winter.

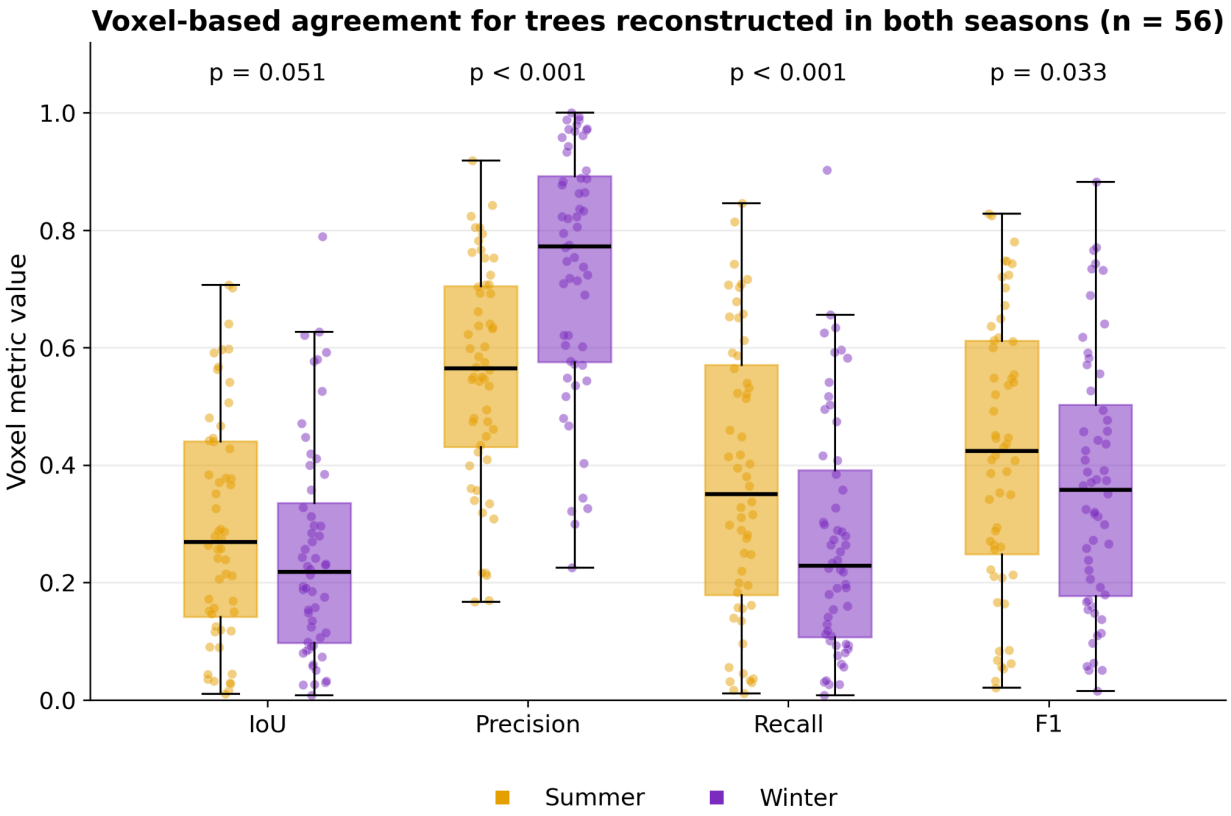


Figure 3: Winter reconstructions were geometrically more precise but less complete than summer reconstructions, resulting in lower overall voxel agreement. Seasonal comparison of voxel-based geometric agreement for the 56 trees successfully reconstructed are shown during both summer and winter. Points represent individual trees; boxes show the interquartile range, horizontal lines indicate the median, and whiskers extend to 1.5 times the interquartile range. Metrics were calculated after discretising the TLS and TLS-scaled Luma AI point clouds onto a common 0.10 m voxel grid. Seasonal differences were evaluated using paired two-sided Wilcoxon signed-rank tests. Winter reconstructions exhibited higher precision but lower recall, IoU and F1 than summer reconstructions.

3.3. Structural metric agreement

Agreement between TLS and TLS-scaled Luma AI estimates was consistently stronger for tree height than for crown area (Figure 4). Height estimates exhibited strong agreement during both summer (CCC = 0.887, n = 63) and winter (CCC = 0.866, n = 66), with little seasonal difference in the strength of agreement. Crown-area agreement was lower than height agreement and declined between seasons, from CCC = 0.795 in summer to CCC = 0.643 in winter. TLS-scaled Luma AI generally underestimated tree height, with a mean percentage error of −6.41% in summer and −12.61% in winter. The corresponding mean absolute percentage errors were 10.24% and 13.77%, respectively.

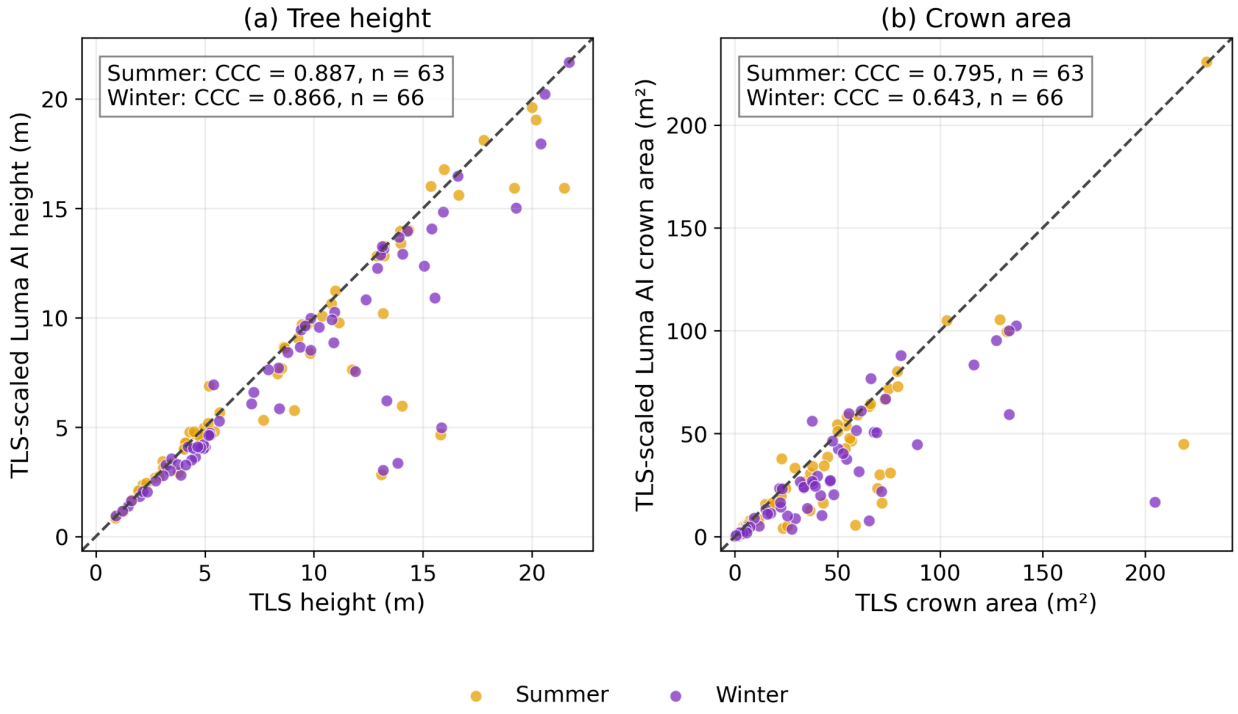
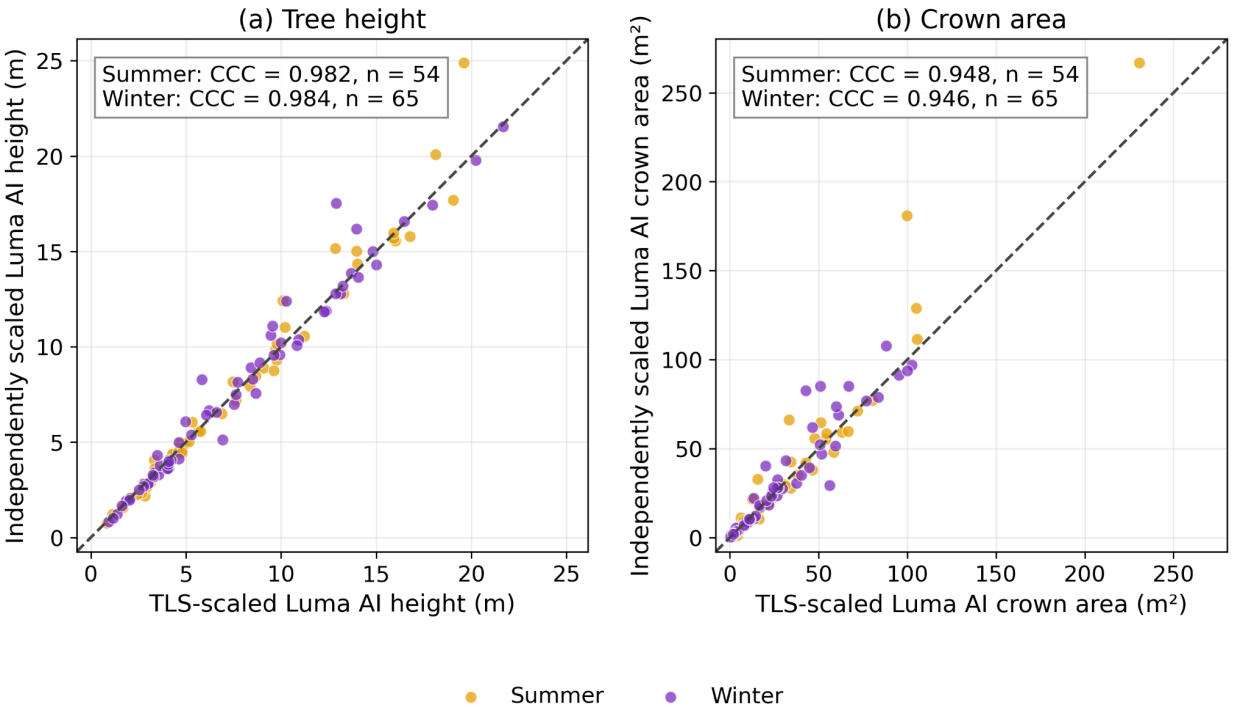


Figure 4: TLS-scaled Luma AI reproduced tree height more consistently than crown area, with crown-area agreement particularly weak during winter. Agreement between TLS-

derived and TLS-scaled Luma AI estimates of (a) tree height and (b) crown area. Orange points represent summer measurements and purple points represent winter measurements. Each point represents one successfully reconstructed tree, and dashed lines indicate perfect 1:1 agreement. Agreement was quantified separately for each season using Lin's concordance correlation coefficient (CCC). Height agreement was consistently strong in both seasons, whereas crown-area agreement was lower, particularly during winter.

Of the 63 usable summer Luma AI reconstructions, 54 contained a successfully reconstructed reference object and could therefore be scaled independently, compared with 65 of the 66 usable winter reconstructions. Thus, the reference object failed to reconstruct or could not be identified more frequently during summer than winter. For trees with measurements available from both scaling procedures, the independently scaled and TLS-scaled Luma AI estimates showed strong agreement. Height CCC was 0.982 in summer (n = 54) and 0.984 in winter (n = 65), while crown-area CCC was 0.948 and 0.946, respectively (Figure 5). The high direct concordance between the two scaling procedures indicates that scaling was not the principal source of disagreement.



406

407 **Figure 5:** Independently scaled and TLS-scaled Luma AI measurements were highly
408 concordant, indicating that the scaling procedure contributed relatively little to differences
409 in the derived structural attributes. Agreement between independently scaled and TLS-
410 scaled Luma AI estimates of (a) tree height and (b) crown area. Orange points represent
411 summer measurements and purple points represent winter measurements. Each point
412 represents a tree for which both scaling procedures were available, and dashed lines
413 indicate perfect 1:1 agreement. The two scaling procedures showed high concordance
414 for both structural metrics in summer and winter.

415 3.4. Competition and Luma AI performance

416 Plot-level competition was not associated with reconstruction failure. Failure rate did not
417 increase significantly with the number of trees in the plot in either summer (Spearman's

ρ = −0.493, p = 0.073) or winter (ρ = −0.033, p = 0.910). Similarly, failure rate was unrelated to total TLS-derived crown area during summer (ρ = −0.098, p = 0.739) or winter (ρ = −0.012, p = 0.968).

Plot-level competition was associated with poorer Luma AI performance during summer but not during winter. Summer plot-level mean voxel F1 decreased as the number of trees in the plot increased (Spearman's ρ = −0.677, p = 0.011; Figure 6). A similar negative association was observed between plot-level mean voxel F1 and total TLS-derived crown area (ρ = −0.692, p = 0.009). Thus, summer trees located in plots containing more trees or greater cumulative crown cover generally exhibited poorer voxel-level agreement with TLS.

Competition was associated with voxel-level reconstruction quality during summer, although its relationship with structural measurement error was weaker. The number of trees in the plot showed a positive but non-significant association with mean absolute percentage error in height (Spearman's ρ = 0.518, p = 0.070) and crown area (ρ = 0.487, p = 0.092). Total TLS-derived crown area was also not significantly associated with either mean height error (ρ = 0.489, p = 0.090) or crown-area error (ρ = 0.330, p = 0.271). Thus, denser summer vegetation was clearly associated with poorer voxel-level agreement, whereas evidence that competition affected the accuracy of the derived height and crown-area measurements was weaker. The absolute percentage error in height or crown area was also not significantly related to the height or crown area of the individual tree in either season (Figure S8).

In winter, neither the number of trees in the plot nor total TLS crown area was significantly associated with plot mean voxel F1, height error or crown-area error. These results indicate that surrounding vegetation had a stronger influence on Luma AI reconstruction performance during leaf-on summer conditions, whereas the effect of plot-level competition was substantially reduced during winter.

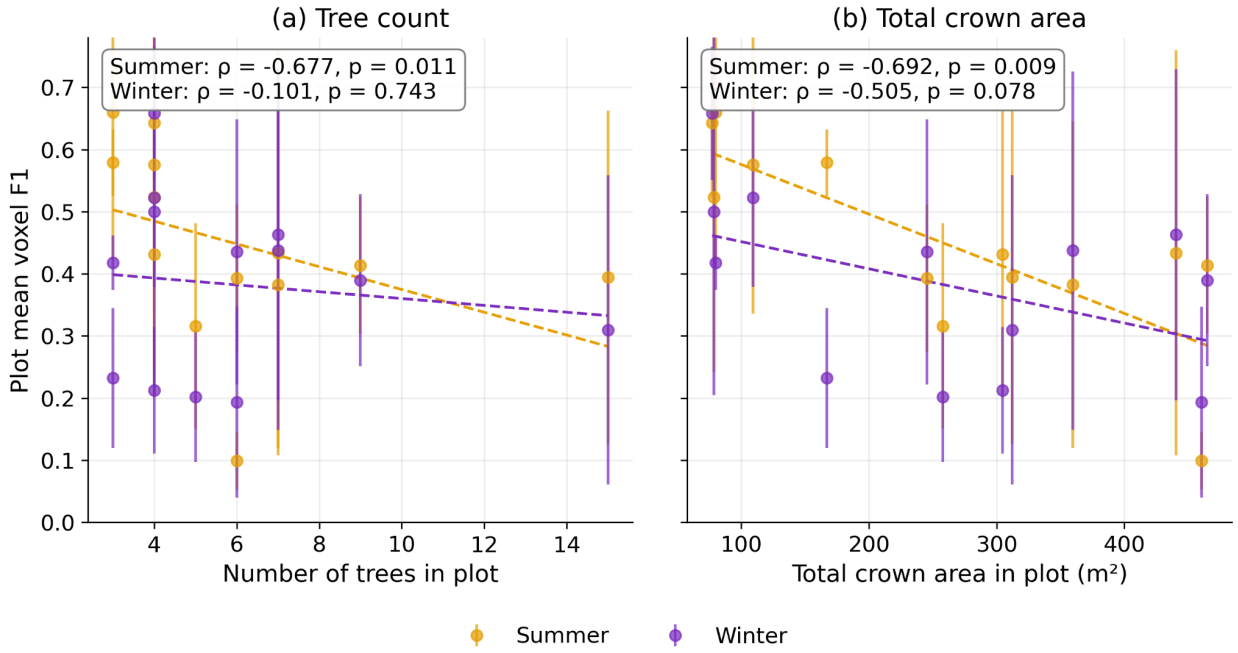


Figure 6: Greater plot-level competition was associated with poorer Luma AI reconstruction performance during summer but not during winter. Relationships between plot-level competition and TLS-scaled Luma AI reconstruction performance during summer and winter. Competition was represented by (a) the number of trees in the plot and (b) their total TLS-derived crown area within each 20 m × 20 m plot. Points show the mean voxel F1 of the successfully reconstructed trees in each plot, and error bars show the corresponding standard deviation. The reported coefficients and p-values are from Spearman's rank correlations calculated using plot-level means.

4. Discussion

Accurate measurements of urban-tree structure are needed to quantify biomass, carbon storage and climate-regulating functions and to support tree management(Wilkes et al. 2018; Pretzsch et al. 2023; Daelman et al. 2026). However, existing approaches involve trade-offs between spatial coverage, structural detail, cost and accessibility (D'hont et al. 2024). We therefore evaluated whether 3D reconstructions generated from smartphone videos using a freely accessible, consumer-facing radiance-field application could provide sufficiently accurate measurements for quantitative urban-tree monitoring. Validating such tools is a critical step toward empowering citizen science and participatory monitoring in urban forestry (Bancks et al. 2018). Luma AI successfully reconstructed most target trees in both seasons and produced quantitatively useful tree-level structural measurements when focal trees were clearly visible and captured with sufficient image overlap. Agreement with TLS was stronger for tree height than for crown area, consistent with previous NeRF studies of saplings and trees (Arshad et al. 2024; Huang et al. 2023; Tian et al. 2025; Muñoz-Bañón et al. 2026). Measurement accuracy was influenced more strongly by plot density than by target-tree size, indicating that even large trees can be measured where surrounding vegetation does not substantially obstruct image acquisition. These findings extend the potential application of smartphone reconstruction beyond urban parks to naturally open ecosystems, including savannas, open woodlands and agroforestry systems, where it could support more frequent and spatially extensive monitoring at a fraction of the cost of repeated TLS surveys.

Seasonal performance in our study was more complex than expected. Although we anticipated that leaf-off conditions would improve reconstruction by reducing crown occlusion(Calders et al. 2015), summer models had higher voxel F1, IoU and recall, whereas winter models had higher precision. One possible explanation is that summer foliage provided relatively large, continuous regions for feature matching, whereas thin leafless branches were more prone to omission. Photogrammetric reconstruction of small and thin plant structures commonly produces holes and incomplete models, and increasing camera distance reduces the image resolution available for reconstructing fine features (Mach et al. 2025; Scher et al. 2019). Furthermore, movement between overlapping images can further disrupt feature matching (Iglhaut et al. 2019). Differences in the TLS reference may have accentuated this pattern: winter TLS captured fine branches concealed by summer foliage(S. Chen et al. 2025), producing a more complete reference. Lower winter F1 may therefore reflect both incomplete smartphone reconstruction and greater representation of fine structure in the winter TLS data. Correspondingly, the larger woody structures recovered by Luma AI generally matched TLS, resulting in high precision, while many finer branches were absent.

Seasonality also influenced the effect of competition on the reconstruction fidelity. During the summer, neighbouring foliage and overlapping crowns restricted visibility and image overlap, causing voxel agreement to decrease with plot density (Petrovska and Jutzi 2025). During the winter, thin exposed branches were difficult to reconstruct in both open and dense plots (Maté-González et al. 2025; Mach et al. 2025), reducing the contrast between competition levels. Vertical F1 profiles confirmed that agreement was generally highest near the lower stem and declined with height, particularly where surrounding

vegetation restricted visibility (Figures S7 and S9). Smartphone reconstruction may therefore support branch-scale measurements for short, unobstructed trees (as evidenced in saplings (Muñoz-Bañón et al. 2026)), whereas fine branch-level geometric and topological traits remain less reliable for tall trees (> 5m) and trees in dense settings with limited overlapping camera viewpoints (Hartley et al. 2024; Scher et al. 2019).

Despite having an impact on overall reconstruction fidelity, competition was only weakly related to errors in the derived height and crown-area measurements, partly because these aggregate attributes can remain reasonably accurate despite the loss of fine geometric detail. This interpretation is consistent with evidence that photogrammetric tree models can reproduce broader tree structure while omitting thin distal branches and underrepresenting the full crown extent (Scher et al. 2019). Limitations in how competition was defined may also have weakened these relationships. The number of trees and total crown area represented vegetation density but did not capture other restrictions on image acquisition. For example, fences or walls prevented the operator from recording some trees from all directions in both seasons, causing severely incomplete reconstructions without increasing either competition indicator (Figure S10). Complete image-based reconstruction requires the target to be visible in multiple overlapping images acquired from different viewpoints, and occlusion or restricted camera trajectories can therefore produce missing geometry (Iglhaut et al. 2019). The absence of strong relationships between the competition indicators and structural error should therefore not be interpreted as evidence that accuracy is unaffected by dense neighborhoods. Rather, both vegetation and site accessibility affected the ability to acquire sufficient overlapping views, but only the former was represented by the selected competition variables.

Metric scaling is a general limitation of camera-based 3D reconstruction. Reconstructions generated from images without metric camera information are typically recovered only up to an unknown scale and therefore require an external metric constraint, such as a known distance, calibrated camera movement or reference object (Li and Lan 2019). In this study, independently scaled and TLS-scaled measurements were highly concordant when the reference object was successfully reconstructed. However, the reference was not recoverable in every model, with failures occurring more frequently during summer. Different objects were used between seasons: a 30 cm ruler in summer and a three-dimensional object measuring 33 × 33 × 32.4 cm in winter. The two objects differed in shape and three-dimensional extent, potentially affecting their visibility and reconstruction. The higher summer failure rate may therefore reflect the smaller visual footprint of the ruler, greater foliage occlusion, or both. Known-size objects have similarly been used to recover metric scale in smartphone-based plant NeRF reconstruction (Xu et al. 2026). Future workflows should evaluate reference objects of different sizes and designs and automate scale recovery by detecting an object and calibrating the reconstructed scene using its known dimensions. High-contrast patterns, known geometry and clearly identifiable corners may facilitate this process (Garrido-Jurado et al. 2014).

Geometric fidelity presents a separate challenge. Standard NeRF methods optimise photometric agreement between observed and rendered images and represent scene geometry implicitly through volumetric density (Mildenhall et al. 2020). Consequently, density may be distributed in ways that reproduce image appearance without accurately reconstructing physical surfaces (Wei et al. 2021; Zhu et al. 2023). Standard 3D Gaussian

Splatting similarly prioritises novel-view rendering and does not inherently impose explicit surface constraints (Kerbl et al. 2023). In this study, the strong agreement in tree height and, to a lesser extent, crown area after scaling indicates that Luma AI generally recovered coarse whole-tree dimensions. However, the lower voxel-level agreement shows that the local distribution of reconstructed geometry did not consistently correspond to TLS at finer spatial scales. This mismatch cannot be attributed solely to an inherent geometric limitation of the reconstruction method because voxel F1 was considerably higher for smaller, unobstructed trees, for which the complete structure could be recorded from closer and more overlapping viewpoints. The lower agreement observed for taller trees and those in denser or access-constrained settings therefore probably reflects a combination of geometric uncertainty, incomplete image coverage, occlusion and the reduced image footprint of fine branches. Depth, surface-normal and LiDAR priors can be incorporated into NeRF and Gaussian-splatting pipelines to improve local geometric accuracy(X. Chen et al. 2023; Deng et al. 2022; Turkulainen et al. 2024; Hu et al. 2024), although these capabilities are not necessarily available in consumer-facing applications. Moreover, while such priors can constrain the geometry of observed surfaces, they cannot fully recover tree components that remain occluded or are insufficiently captured across overlapping views in dense vegetation.

Consumer-facing platforms improve accessibility but introduce limitations relating to reproducibility and data governance. Luma AI automates reconstruction without requiring specialist photogrammetric expertise or high-performance computing, but its proprietary, cloud-based workflow prevents users from inspecting the source code or controlling the algorithm and software version (Luma is your creative partner 2026). This limits

reproducibility because software changes can alter analytical results (Ziemann et al. 2023). Cloud processing may also be unsuitable where videos contain identifiable people, private property, culturally sensitive sites or sensitive species locations (Chapman 2020). Locally operated, version-controlled pipelines may therefore be preferable when reproducibility or confidentiality is critical, although they require greater computational resources and expertise. Importantly, the original videos should be retained as the primary research data, allowing observations to be reprocessed using transparent frameworks such as Nerfstudio or future reconstruction methods (Tancik et al. 2023; Wang et al. 2026). Consumer-facing platforms can thus support rapid and accessible processing, while retaining the videos preserves opportunities for reproducible future reanalysis.

Smartphone-based reconstruction occupies a complementary position between conventional field measurements and specialist 3D equipment. TLS remains essential when complete canopy representation and fine-scale geometric accuracy measurements are required. Smartphone video, however, offers a practical way to increase the frequency, spatial coverage and wider participation of ecological monitoring. TLS could provide periodic calibration and validation, while smartphone videos could support repeated observations across larger numbers of trees and sites. Future studies should test this approach across a wider range of ecosystems, species, crown architectures, and environmental conditions, while evaluating automated scaling, DBH extraction, repeat-survey sensitivity and the reliability of finer branch-level traits. These developments should not be considered solely within the context of NeRF, because image-based three-dimensional reconstruction is advancing rapidly through radiance fields, Gaussian-

splatting approaches (Rangelov et al. 2024) and other emerging scene-reconstruction methods (Belkaid et al. 2024; Barberteguy et al. 2026; Wang et al. 2026). Ecological monitoring may not always be able to adopt each new computational method as it appears, but field data collection can be designed to benefit from future developments. Consistently acquired and archived smartphone videos provide a particularly valuable input because they can be collected using hardware already available to most participants and reanalysed repeatedly as algorithms improve. Our study therefore shows not only that a free consumer-facing application can produce ecologically meaningful measurements, but also that ordinary smartphone videos can form a reusable foundation for future 3D ecological monitoring.

Competing Interest Statement

Authors declare no competing interest.

Declaration on the Use of AI

The authors used ChatGPT to assist in improving the clarity of writing. The authors also used ChatGPT to assist with coding during the development and refinement of analysis scripts. AI tools were not used to conceive the research ideas, interpret the results, or draw the conclusions. The authors reviewed and verified all the AI outputs. The authors take full responsibility for the accuracy and reproducibility of the work. All AI-assisted codes used in the study will be made available in the repository listed in the Data Availability statement.

References

Aronson, Myla F. J., Christopher A. Lepczyk, Karl L. Evans, et al. 2017. “Biodiversity in the City: Key Challenges for Urban Green Space Management.” *Frontiers in Ecology and the Environment* 15 (4): 189–196.

Arshad, Muhammad Arbab, Talukder Jubery, James Afful, et al. 2024. “Evaluating Neural Radiance Fields for 3D Plant Geometry Reconstruction in Field Conditions.” *Plant Phenomics (Washington, D.C.)* 6 (0235): 0235.

Bancks, Nick, Eric A. North, and Gary R. Johnson. 2018. “An Analysis of Agreement between Volunteer- and Researcher-Collected Urban Tree Inventory Data.” *Arboriculture & Urban Forestry* 44 (2): 73–86.

Barberteguy, Victor, Ahmet Iscen, Mathilde Caron, Alireza Fathi, Gül Varol, and Cordelia Schmid. 2026. “Pano3D: Unified 3D Reconstruction and Panoptic Segmentation.” In *arXiv [cs.CV]*. June 12. arXiv. https://doi.org/10.48550/arXiv.2606.14307.

Belkaid, Maryem, El Arbi Abdellaoui Alaoui, Mostafa Merras, Achraf Berrajaa, and Nabil El Akkad. 2024. “Review of 3D Scene Reconstruction: From Traditional Methods to Advanced Deep Learning Models.” *2024 3rd International Conference on Embedded Systems and Artificial Intelligence (ESAI)*, December 19, 1–11.

Bertram, Christine, and Katrin Rehdanz. 2015. “The Role of Urban Green Space for Human Well-Being.” *Ecological Economics: The Journal of the International Society*

for Ecological Economics 120 (December): 139–152.

Calders, K., J. Adams, J. Armston, and H. Bartholomeus. 2020. “Terrestrial Laser Scanning in Forest Ecology: Expanding the Horizon.” *Remote Sensing of Environment*. https://www.sciencedirect.com/science/article/pii/S0034425720304752.

Calders, K., G. Newnham, and A. Burt. 2015. “Nondestructive Estimates of Above-ground Biomass Using Terrestrial Laser Scanning.” *Methods in Ecology and Evolution / British Ecological Society*. https://besjournals.onlinelibrary.wiley.com/doi/abs/10.1111/2041-210X.12301.

Cerbone, H., S. M. K. Moorthy, and R. Salguero-Gomez. 2025. *Democratizing 3D Ecology: Mobile Neural Radiance Field for Scalable Ecosystem Mapping in Change Detection*. https://ecoevorxiv.org/repository/view/9505/.

Chapman, Arthur. 2020. *Current Best Practices for Generalizing Sensitive Species Occurrence Data*. https://doi.org/10.15468/DOC-5JP4-5G10.

Chen, Shilin, Hans Verbeeck, Louise Terryn, et al. 2025. “The Impact of Leaf-Wood Separation Algorithms on Aboveground Biomass Estimation from Terrestrial Laser Scanning.” *Remote Sensing of Environment* 318 (114581): 114581.

Chen, Xuanzhu, Zhenbo Song, Jun Zhou, Dong Xie, and Jianfeng Lu. 2023. “Camera and LiDAR Fusion for Urban Scene Reconstruction and Novel View Synthesis via Voxel-Based Neural Radiance Fields.” *Remote Sensing* 15 (18): 4628.

Chen, Zhao, Lingnan Dai, Dianchang Wang, Qian Guo, and Rong Zhao. 2025. “FS-MVSNet: A Multi-View Image-Based Framework for 3D Forest Reconstruction and Parameter Extraction of Single Trees.” *Forests* 16 (6): 927.

Cherlet, Wout, Karun Dayal, Shilin Chen, et al. 2026. “Benchmarking Tree Instance Segmentation of Terrestrial Laser Scanning Point Clouds.” *ISPRS Journal of Photogrammetry and Remote Sensing: Official Publication of the International Society for Photogrammetry and Remote Sensing (ISPRS)* 231 (January): 230–247.

Daelman, Todi, Matthias Demuzere, Frieke Vancoillie, et al. 2026. “The Influence of Urban and Tree Morphology on Modeled Daytime Mean Radiant Temperature.” *Urban Climate* 68 (103000): 103000.

Das, Sumanta, Malini Roy Choudhury, Bhagyasree Chatterjee, et al. 2024. “Unraveling the Urban Climate Crisis: Exploring the Nexus of Urbanization, Climate Change, and Their Impacts on the Environment and Human Well-Being - A Global Perspective.” *AIMS Public Health* 11 (3): 963–1001.

Davenport, Ian, Peter J. Lawrence, Emily R. Lines, and Simon J. Carr. 2026. “Intra- and Interspecific Variations of Tree Allometry in Rural and Urban Settings.” *Urban Forestry & Urban Greening* 125 (129687): 129687.

Deng, Kangle, Andrew Liu, Jun-Yan Zhu, and Deva Ramanan. 2022. “Depth-Supervised NeRF: Fewer Views and Faster Training for Free.” *2022 IEEE/CVF Conference on Computer Vision and Pattern Recognition (CVPR)*, June, 12872–

12881.

D'hont, B., K. Calders, H. Bartholomeus, et al. 2024. "Evaluating Airborne, Mobile and Terrestrial Laser Scanning for Urban Tree Inventories: A Case Study in Ghent, Belgium." *Urban Forestry & Urban Greening* 99 (128428): 128428.

Dong, Xinyu, Yanmei Ye, Dan Su, et al. 2025. "Adaptive Ranking of Specific Tree Species for Targeted Green Infrastructure Intervention in Response to Urban Hazards." *Urban Forestry & Urban Greening* 107 (128776): Not Available.

Douglas, Owen, Mick Lennon, and Mark Scott. 2017. "Green Space Benefits for Health and Well-Being: A Life-Course Approach for Urban Planning, Design and Management." *Cities (London, England)* 66 (June): 53–62.

Drénou, Christophe, Marine Bouvier, and Jean Lemaire. 2015. "The Diagnostic Method ARCHI Applied on Declining Pedunculate Oaks." *Arboricultural Journal* 37 (3): 166–179.

Feng, Boyu, Ying Zhang, and Robin Bourke. 2021. "Urbanization Impacts on Flood Risks Based on Urban Growth Data and Coupled Flood Models." *Natural Hazards (Dordrecht, Netherlands)* 106 (1): 613–627.

Garrido-Jurado, S., R. Muñoz-Salinas, F. J. Madrid-Cuevas, and M. J. Marín-Jiménez. 2014. "Automatic Generation and Detection of Highly Reliable Fiducial Markers under Occlusion." *Pattern Recognition* 47 (6): 2280–2292.

Gaston, Kevin J., and Masashi Soga. 2020. "Extinction of Experience: The Need to Be

More Specific.” *People and Nature (Hoboken, N.J.)* 2 (3): 575–581.

Ghanbari Parmehr, Ebadat, and Marco Amati. 2021. “Individual Tree Canopy Parameters Estimation Using UAV-Based Photogrammetric and LiDAR Point Clouds in an Urban Park.” *Remote Sensing* 13 (11): 2062.

Giaquinto, Alessia, Giampaolo Ferraioli, and Silvio Del Pizzo. 2026. “Evaluating Neural Radiance Fields for Image-Based 3D Reconstruction: A Comparative Study with SfM-MVS.” *Geomatics (Basel, Switzerland)* 6 (1): 4.

Girardeau-Montaut, Daniel. 2016. “CloudCompare.” *France: EDF R&D Telecom ParisTech* 11: 5.

Hald-Mortensen, Christian. 2023. “The Main Drivers of Biodiversity Loss: A Brief Overview.” *Journal of Ecology and Natural Resources* 7 (3): 000346.

Hartley, Robin J. L., Sadeepa Jayathunga, Justin Morgenroth, and Grant D. Pearse. 2024. “Tree Branch Characterisation from Point Clouds: A Comprehensive Review.” *Current Forestry Reports*, ahead of print, July 25. https://doi.org/10.1007/s40725-024-00225-5.

Howie, Noah A., and Andrea De Stefano. 2024. “Measuring Tree Diameter Using LiDAR Equipped iPad: An Evaluation of ForestScanner and Arboreal Forest Applications.” *Forest Science* 70 (4): 304–310.

Hu, Kewei, Wei Ying, Yaoqiang Pan, Hanwen Kang, and Chao Chen. 2024. “High-Fidelity 3D Reconstruction of Plants Using Neural Radiance Fields.” *Computers*

and Electronics in Agriculture 220 (108848): 108848.

Iglhaut, Jakob, Carlos Cabo, Stefano Puliti, Livia Piermattei, James O'Connor, and Jacqueline Rosette. 2019. "Structure from Motion Photogrammetry in Forestry: A Review." *Current Forestry Reports* 5 (3): 155–168.

Kerbl, Bernhard, Georgios Kopanas, Thomas Leimkühler, and George Drettakis. 2023. "3D Gaussian Splatting for Real-Time Radiance Field Rendering." In *arXiv [cs.GR]*. August 8. arXiv. https://doi.org/10.48550/arXiv.2308.04079.

Lachenbruch, Peter A. 2014. "McNemar Test." In *Wiley StatsRef: Statistics Reference Online*. John Wiley & Sons, Ltd, September 29. https://doi.org/10.1002/9781118445112.stat04876.

Li, Langping, and Hengxing Lan. 2019. "Recovering Absolute Scale for Structure from Motion Using the Law of Free Fall." *Optics and Laser Technology* 112 (April): 514–523.

Lindberg, Eva, and Johan Holmgren. 2017. "Individual Tree Crown Methods for 3D Data from Remote Sensing." *Current Forestry Reports* 3 (1): 19–31.

Lin, L. I. 1989. "A Concordance Correlation Coefficient to Evaluate Reproducibility." *Biometrics* 45 (1): 255–268.

Li, Xuecao, Yuyu Zhou, Jiyong Eom, Sha Yu, and Ghassem R. Asrar. 2019. "Projecting Global Urban Area Growth through 2100 Based on Historical Time Series Data and Future Shared Socioeconomic Pathways." *Earth's Future* 7 (4): 351–362.

Luma Is Your Creative Partner. 2026. Luma. https://lumalabs.ai/.

Mach, Jiří, Zdeněk Svatý, Ondřej Šoupa, Luboš Nouzovský, and Martin Halecký. 2025. "Implementation of an SfM-MVS-Based Photogrammetry Approach for Detailed 3D Reconstruction of Plants." *Plant Methods* 21 (1): 127.

Maeda, Eduardo Eiji, Benjamin Brede, Kim Calders, et al. 2025. "Expanding Forest Research with Terrestrial LiDAR Technology." *Nature Communications* 16 (1): 8853.

Maté-González, Miguel Ángel, Roy Yali, Jesús Rodríguez-Hernández, Enrique González-González, and Julián Aguirre de Mata. 2025. "Comparison of NeRF- and SfM-Based Methods for Point Cloud Reconstruction for Small-Sized Archaeological Artifacts." *Remote Sensing* 17 (14): 2535.

Mildenhall, Ben, Pratul P. Srinivasan, Matthew Tancik, Jonathan T. Barron, Ravi Ramamoorthi, and Ren Ng. 2020. "NeRF: Representing Scenes as Neural Radiance Fields for View Synthesis." In *Lecture Notes in Computer Science*. Lecture Notes in Computer Science. Springer International Publishing.

Miller, Jordan, Justin Morgenroth, and Christopher Gomez. 2015. "3D Modelling of Individual Trees Using a Handheld Camera: Accuracy of Height, Diameter and Volume Estimates." *Urban Forestry & Urban Greening* 14 (4): 932–940.

Mokroš, Martin, Tomáš Mikita, Arunima Singh, et al. 2021. "Novel Low-Cost Mobile Mapping Systems for Forest Inventories as Terrestrial Laser Scanning Alternatives." *International Journal of Applied Earth Observation and*

Geoinformation: ITC Journal 104 (102512): 102512.

Moore, Melinda, Philip Gould, and Barbara S. Keary. 2003. “Global Urbanization and Impact on Health.” *International Journal of Hygiene and Environmental Health* 206 (4-5): 269–278.

Muñoz-Bañón, Miguel Ángel, Nived Chebrolu, Sruthi M. Krishna Moorthy, et al. 2026. “Sapling-NeRF: Geo-Localised Sapling Reconstruction in Forests for Ecological Monitoring.” In *arXiv [cs.RO]*. February 26. arXiv. https://doi.org/10.48550/arXiv.2602.22731.

Nowak, David J., and Daniel E. Crane. 2002. “Carbon Storage and Sequestration by Urban Trees in the USA.” *Environmental Pollution (Barking, Essex: 1987)* 116 (3): 381–389.

Parker, David E. 2010. “Urban Heat Island Effects on Estimates of Observed Climate Change: Urban Heat Island Effects on Estimates of Observed Climate Change.” *Wiley Interdisciplinary Reviews. Climate Change* 1 (1): 123–133.

Petrovska, Ivana, and Boris Jutzi. 2025. “Seeing beyond Vegetation: A Comparative Occlusion Analysis between Multi-View Stereo, Neural Radiance Fields and Gaussian Splatting for 3D Reconstruction.” *ISPRS Open Journal of Photogrammetry and Remote Sensing* 16 (100089): 100089.

Pretzsch, H., A. Moser-Reischl, M. A. Rahman, S. Pauleit, and T. Rötzer. 2023. “Towards Sustainable Management of the Stock and Ecosystem Services of Urban Trees. From Theory to Model and Application.” *Trees (Berlin, Germany: West)* 37

(1): 177–196.

Rangelov, Dimitar, Sierd Waanders, Kars Waanders, Maurice van Keulen, and Radoslav Miltchev. 2024. “Impact of Camera Settings on 3D Reconstruction Quality: Insights from NeRF and Gaussian Splatting.” *Sensors (Basel, Switzerland)* 24 (23): 7594.

Roberts, John, Andrew Koeser, Amr Abd-Elrahman, et al. 2019. “Mobile Terrestrial Photogrammetry for Street Tree Mapping and Measurements.” *Forests* 10 (8): 701.

Sadeghian, Hamed, Hamed Naghavi, Rahim Maleknia, Javad Soosani, and Norbert Pfeifer. 2022. “Estimating the Attributes of Urban Trees Using Terrestrial Photogrammetry.” *Environmental Monitoring and Assessment* 194 (9): 625.

Scher, C. Lane, Emily Griffoul, and Charles H. Cannon. 2019. “Drone-Based Photogrammetry for the Construction of High-Resolution Models of Individual Trees.” *Trees (Berlin, Germany: West)* 33 (5): 1385–1397.

Seamans, G. S. 2013. “Mainstreaming the Environmental Benefits of Street Trees.” *Urban Forestry & Urban Greening*. https://www.sciencedirect.com/science/article/pii/S161886671200091X.

Seto, Karen C., Burak Güneralp, and Lucy R. Hutyra. 2012. “Global Forecasts of Urban Expansion to 2030 and Direct Impacts on Biodiversity and Carbon Pools.” *Proceedings of the National Academy of Sciences of the United States of America* 109 (40): 16083–16088.

794 Sicard, Pierre, Evgenios Agathokleous, Susan C. Anenberg, Alessandra De Marco,
795 Elena Paoletti, and Vicent Calatayud. 2023. “Trends in Urban Air Pollution over the
796 Last Two Decades: A Global Perspective.” *The Science of the Total Environment*
797 858 (Pt 2): 160064.

798 Suárez, Juan C., Carlos Ontiveros, Steve Smith, and Stewart Snape. 2005. “Use of
799 Airborne LiDAR and Aerial Photography in the Estimation of Individual Tree Heights
800 in Forestry.” *Computers & Geosciences* 31 (2): 253–262.

801 Tancik, Matthew, Ethan Weber, Evonne Ng, et al. 2023. “Nerfstudio: A Modular
802 Framework for Neural Radiance Field Development.” In *arXiv [cs.CV]*. February 8.
803 arXiv. https://doi.org/10.48550/arXiv.2302.04264.

804 Tatsumi, Shinichi, Keiji Yamaguchi, and Naoyuki Furuya. 2023. “ForestScanner: A
805 Mobile Application for Measuring and Mapping Trees with LiDAR-equipped iPhone
806 and iPad.” *Methods in Ecology and Evolution* 14 (7): 1603–1609.

807 Taylor, Jonathon, Charles Simpson, Oscar Brousse, Anna-Kaisa Viitanen, and Clare
808 Heaviside. 2024. “The Potential of Urban Trees to Reduce Heat-Related Mortality
809 in London.” *Environmental Research Letters* 19 (5): 054004.

810 Terryn, Louise, Kim Calders, Félicien Meunier, et al. 2024. “New Tree Height
811 Allometries Derived from Terrestrial Laser Scanning Reveal Substantial
812 Discrepancies with Forest Inventory Methods in Tropical Rainforests.” *Global*
813 *Change Biology* 30 (8): e17473.

814 Threlfall, Caragh G., Luis Mata, Jessica A. Mackie, et al. 2017. “Increasing Biodiversity

in Urban Green Spaces through Simple Vegetation Interventions." *The Journal of Applied Ecology* 54 (6): 1874–1883.

Tsuzuki, Yamato, and Akio Inoue. 2026. "Measuring Tree Diameter at Breast Height in Urban Green Spaces Using ForestScanner: Implications for Citizen Science." *Urban Forestry & Urban Greening* 118 (129293): 129293.

Turkulainen, Matias, Xuqian Ren, Iaroslav Melekhov, Otto Seiskari, Esa Rahtu, and Juho Kannala. 2024. "DN-Splatter: Depth and Normal Priors for Gaussian Splatting and Meshing." In *arXiv [cs.CV]*. March 26. arXiv. https://doi.org/10.48550/arXiv.2403.17822.

United Nations Department for Economic and Social Affairs. 2020. *World Urbanization Prospects 2018: Highlights: Highlights*. Population Studies 421. United Nations.

Vanage, Shreyas. 2025. "Mobile Market Analysis: Exploring iOS and Android Trends, User Growth and Platform Competition (2011-2023)." *User Growth and Platform Competition (2011-2023)(July 01, 2025)*. https://papers.ssrn.com/sol3/papers.cfm?abstract_id=5333043.

Výbošťok, Jozef, Juliána Chudá, Michal Skladan, Arunima Singh, Daniel Tomčík, and Martin Mokroš. 2025. "Efficient and Cost-Effective Monitoring of Urban Green Spaces Using Combination of Photogrammetry, LiDAR, and RTK in an iPhone-Based Approach." *Central European Forestry Journal* 71 (3): 207–223.

Výbošťok, Jozef, Juliána Chudá, Daniel Tomčík, et al. 2025. "An Open and Novel Low-Cost Terrestrial Laser Scanner Prototype for Forest Monitoring." *Sensors (Basel,*

Switzerland) 26 (1): 63.

Wang, Jianyuan, Minghao Chen, Shangzhan Zhang, et al. 2026. “VGGT-Ω.” In *arXiv [cs.CV]*. May 14. arXiv. https://doi.org/10.48550/arXiv.2605.15195.

Wei, Yi, Shaohui Liu, Yongming Rao, Wang Zhao, Jiwen Lu, and Jie Zhou. 2021. “NerfingMVS: Guided Optimization of Neural Radiance Fields for Indoor Multi-View Stereo.” In *arXiv [cs.CV]*. September 2. arXiv. https://doi.org/10.48550/arXiv.2109.01129.

Wheeler, Philip, Janice Ansine, and Holly Woo. 2025. “Mapping Social & Cultural Values of Trees with Citizen Science.” Paper presented Urban Tree Festival, 2025, Online webinar. May 16. https://oro.open.ac.uk/109171/.

Wilkes, Phil, Mathias Disney, Matheus Boni Vicari, Kim Calders, and Andrew Burt. 2018. “Estimating Urban above Ground Biomass with Multi-Scale LiDAR.” *Carbon Balance and Management* 13 (1): 10.

Williams, Katie. 2009. “Space per Person in the UK: A Review of Densities, Trends, Experiences and Optimum Levels.” *Land Use Policy* 26 (December): S83–S92.

Woo, Holly, Janice Ansine, and Philip Wheeler. 2024. “Enriching the Treezilla User Experience to See Trees Mapped in Context.” Paper presented Future of UK Treescapes Conference 2024, 2024, Glasgow, Scotland. https://oro.open.ac.uk/109095/.

Xu, Xing, Shangcun Chen, Yu Liu, et al. 2026. “BN-NeRF: A Fast 3D Reconstruction

and Phenotyping Framework for Banana Plants Using Handheld Devices." *Plant Phenomics (Washington, D.C.)* 8 (3): 100230.

Zhang, Fan, and Haochen Qian. 2024. "A Comprehensive Review of the Environmental Benefits of Urban Green Spaces." *Environmental Research* 252 (Pt 2): 118837.

Zhang, Yang, Bing Zhu, Xiaoyu Jiang, Xingpeng Yan, Hairong Hu, and Lei Wang. 2026. "Radiance Field-Based 3D Reconstruction and Potential Applications." *Science China Technological Sciences* 69 (3). https://doi.org/10.1007/s11431-025-3167-1.

Zhu, Bingfan, Yanchao Yang, Xulong Wang, Youyi Zheng, and Leonidas Guibas. 2023. "VDN-NeRF: Resolving Shape-Radiance Ambiguity via View-Dependence Normalization." In *arXiv [cs.CV]*. March 31. arXiv. https://doi.org/10.48550/arXiv.2303.17968.

Ziemann, Mark, Pierre Poulain, and Anusuiya Bora. 2023. "The Five Pillars of Computational Reproducibility: Bioinformatics and beyond." *Briefings in Bioinformatics* 24 (6): bbad375.

A consumer-facing application for radiance field-based 3D reconstruction enables accessible measurement of urban tree structure

Supplementary section



Figure S1: Reference objects used for independent scaling of Luma AI point clouds. Photos and the corresponding reconstructions of the same target tree showing (a) the coloured 30 cm ruler used during summer data collection and (b) the reference cube of known dimensions used during winter data collection.

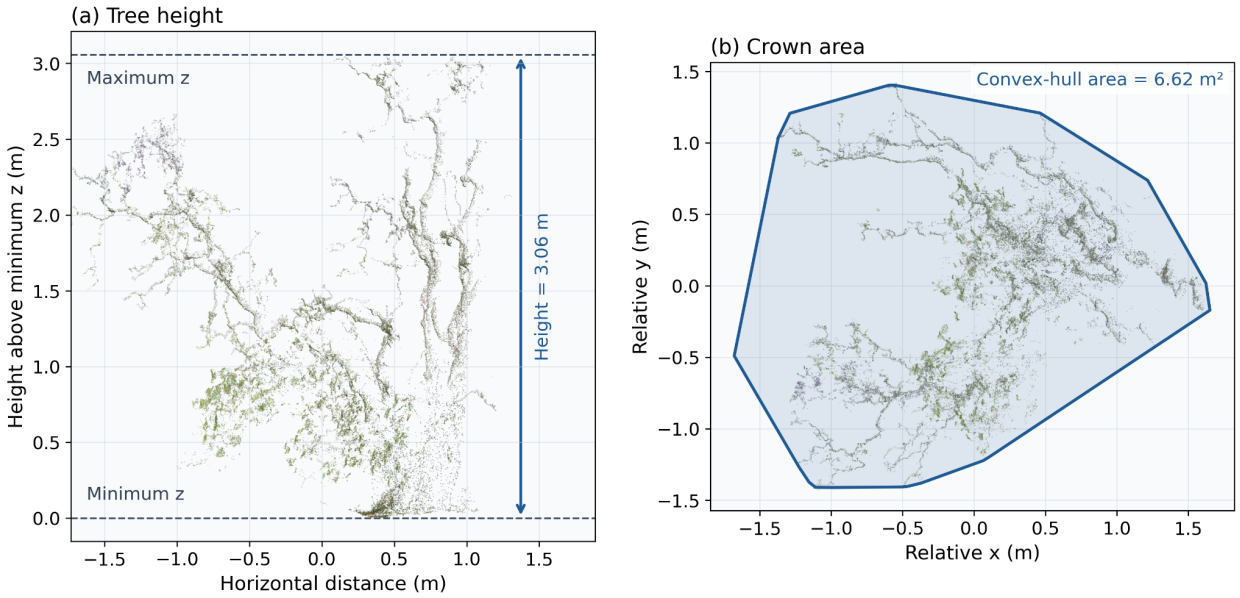


Figure S2: Illustration of the structural metrics extracted from tree-level point clouds. (a) Tree height was calculated as the vertical difference between maximum and minimum z-axis values. (b) Crown area was calculated from the two-dimensional convex hull fitted to the 0.05 m spatially subsampled horizontal projection of the complete tree point cloud. A TLS point cloud from a plot with high density of trees (> 6 trees) is shown as an example.

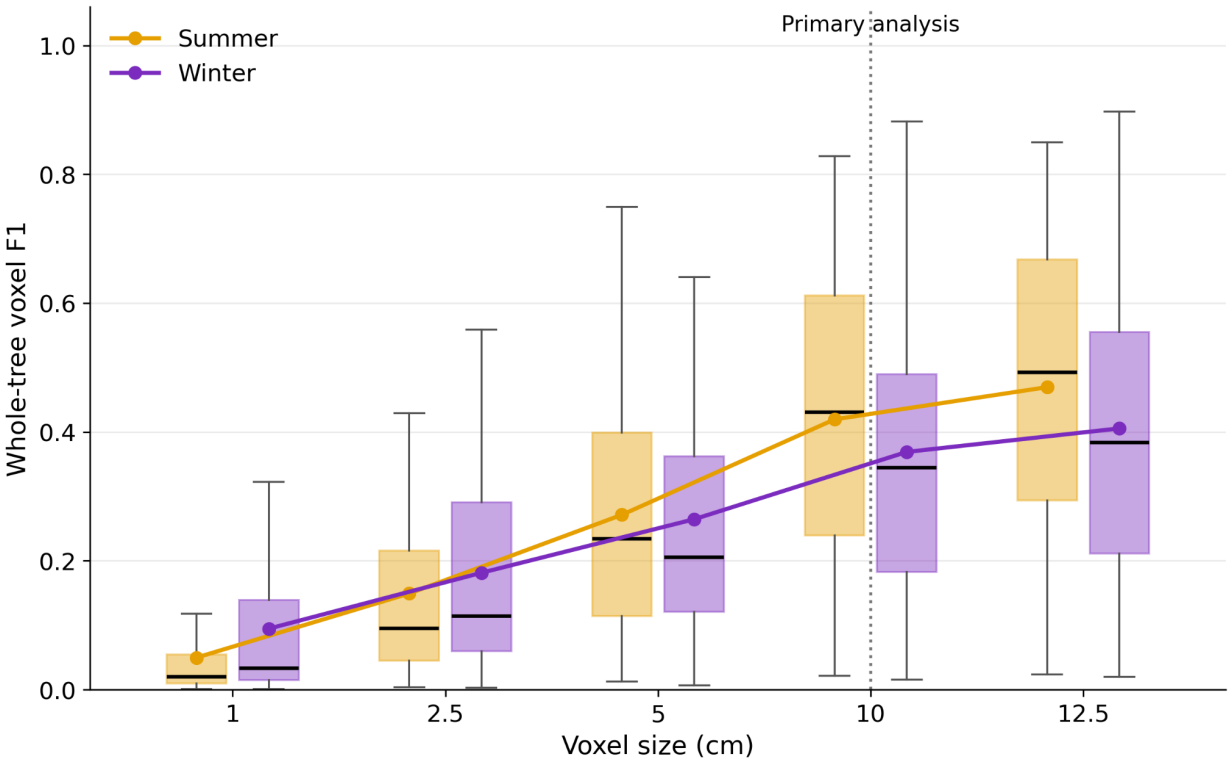


Figure S3: Sensitivity analysis of whole-tree voxel F1 scores across a range of voxel sizes (1–12.5 cm). While the seasonal trend between summer and winter reconstructions becomes consistent from 5 cm onward, F1 scores stabilize beyond the 10 cm threshold. The vertical dotted line denotes the 10 cm voxel size selected in this study to account for co-registration errors between the different point cloud resolutions.

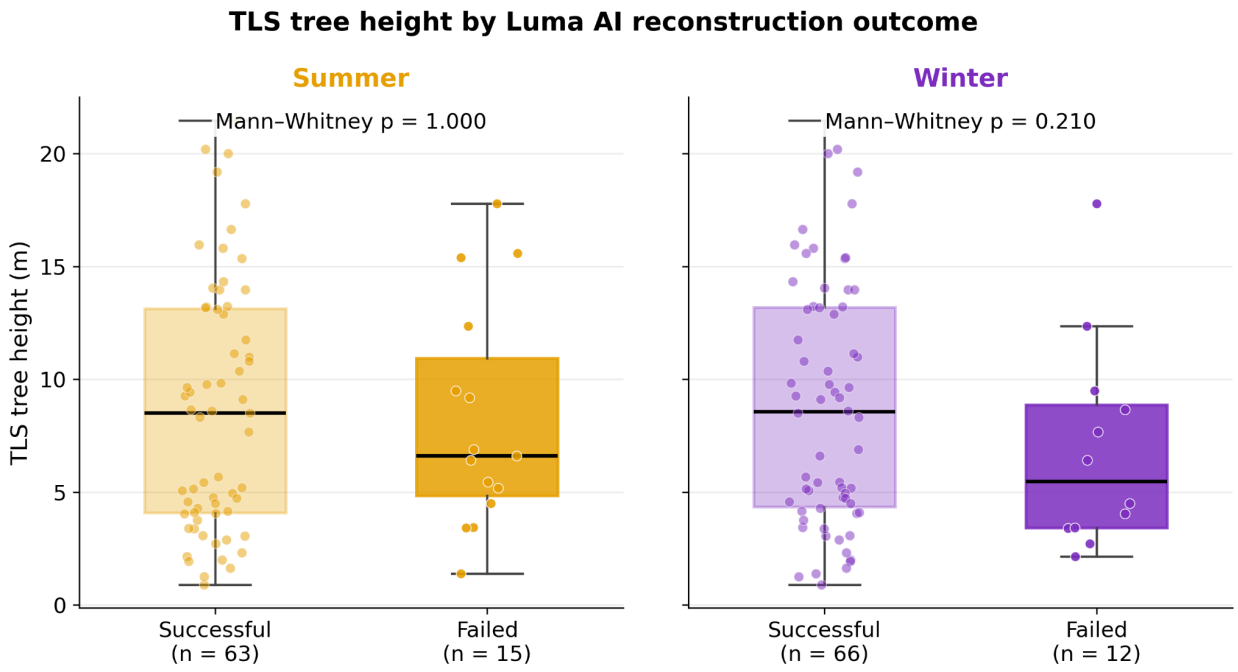
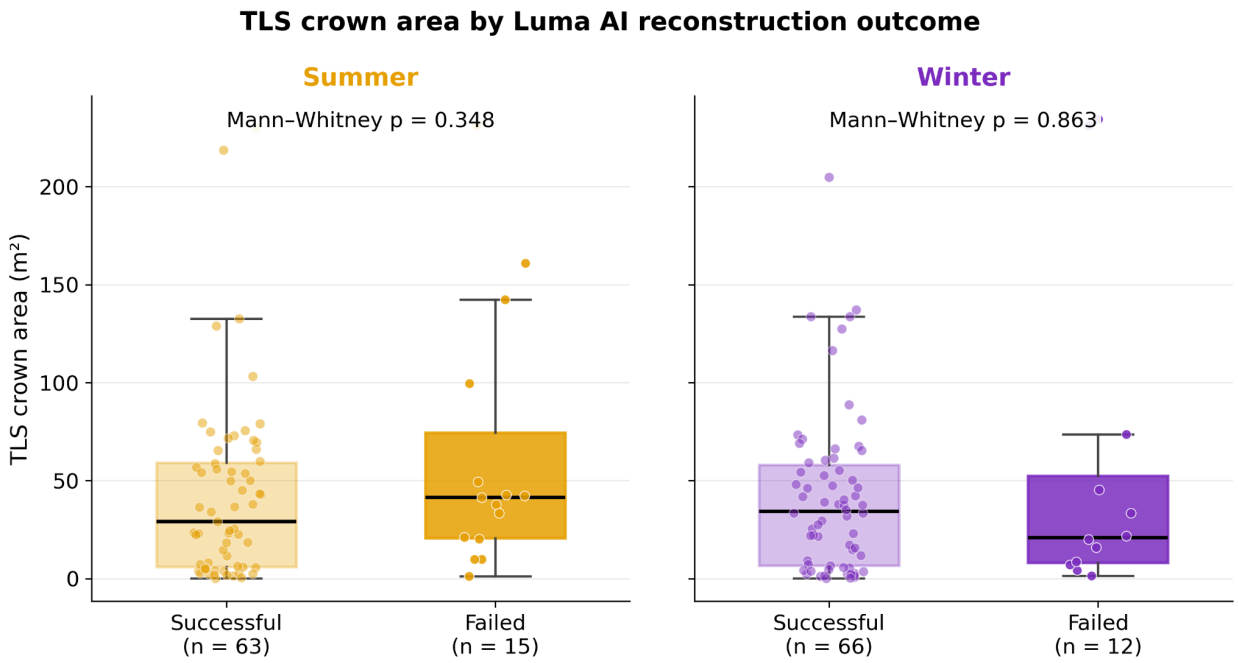
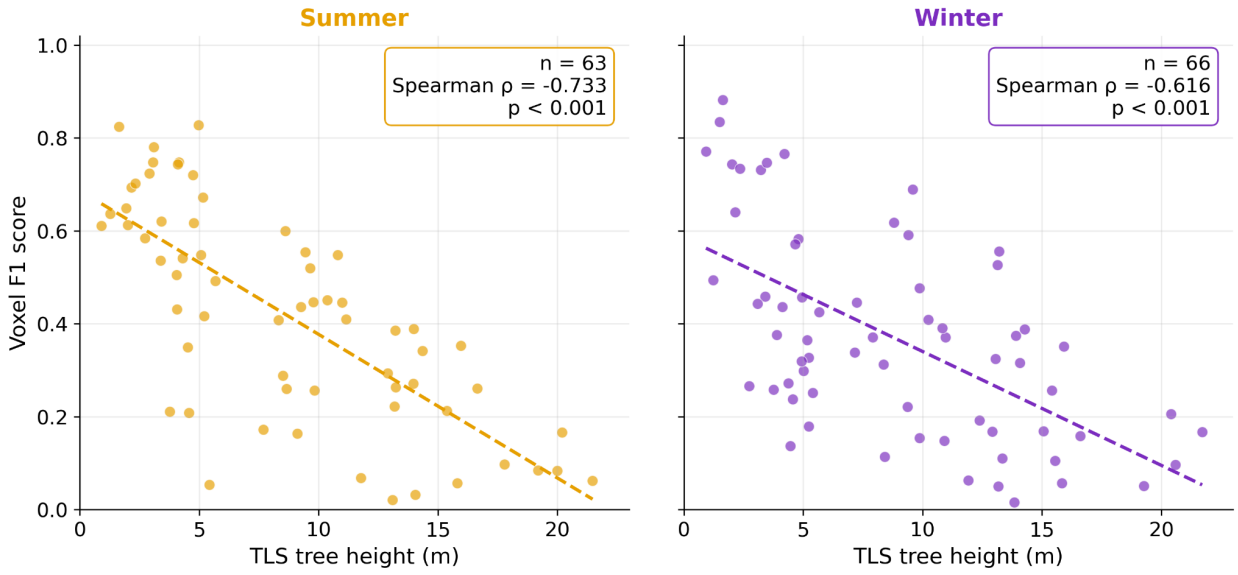


Figure S4: TLS-derived tree height according to Luma AI reconstruction outcome during summer and winter. Points represent individual target trees; boxes show the interquartile range, horizontal lines indicate the median, and whiskers extend to 1.5 times the interquartile range. Differences between successful and failed reconstructions were evaluated separately for each season using two-sided Mann–Whitney U tests. Tree height did not differ significantly between successful and failed reconstructions in either summer ($p = 1.000$) or winter ($p = 0.210$).



905

906 **Figure S5:** TLS-derived crown area according to Luma AI reconstruction outcome during
907 summer and winter. Points represent individual target trees; boxes show the interquartile
908 range, horizontal lines indicate the median, and whiskers extend to 1.5 times the
909 interquartile range. Differences between successful and failed reconstructions were
910 evaluated separately for each season using two-sided Mann–Whitney U tests. Crown
911 area did not differ significantly between successful and failed reconstructions in either
912 summer ($p = 0.348$) or winter ($p = 0.863$).

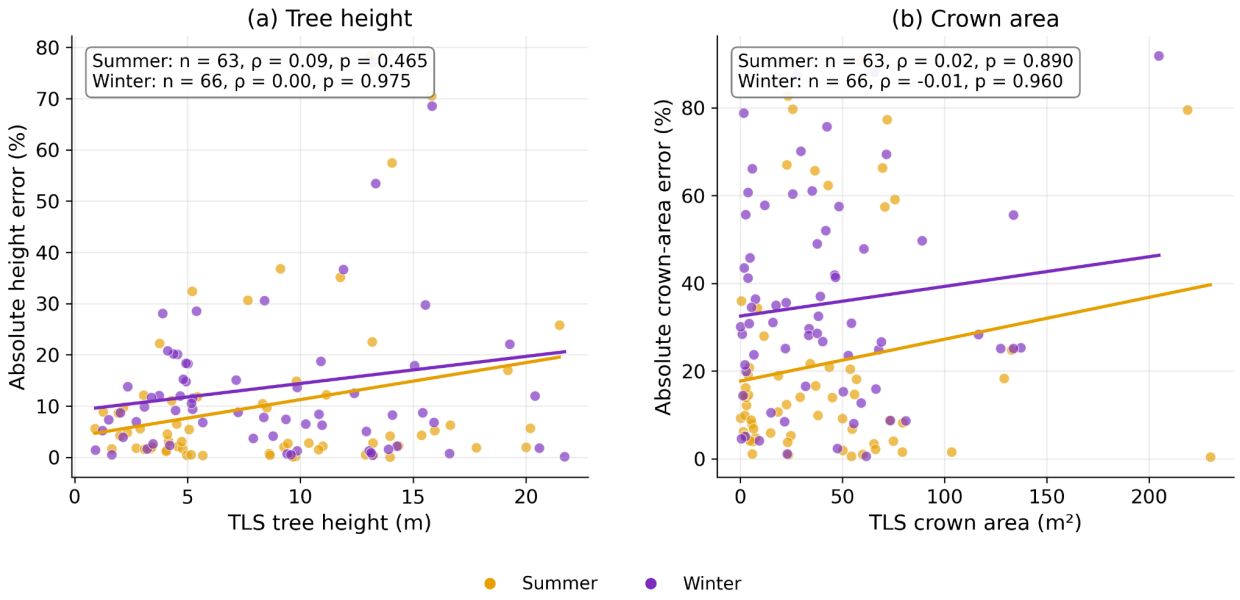


913

914 **Figure S6:** Relationship between TLS-derived tree height and voxel F1 score for TLS-
915 scaled Luma AI reconstructions acquired during summer and winter. Each point
916 represents one successfully reconstructed tree. Voxel F1 was calculated after discretising
917 the TLS and Luma AI point clouds onto a common 0.10 m voxel grid. Dashed lines show
918 least-squares trends for visualisation. Associations were evaluated using Spearman's
919 rank correlation. Voxel F1 decreased significantly with increasing tree height during both
920 summer ($\rho = -0.733$, $p < 0.001$; $n = 63$) and winter ($\rho = -0.616$, $p < 0.001$; $n = 66$).



Figure S7: Vertical distribution of voxel-based F1 agreement between TLS and TLS-scaled Luma AI point clouds for individual trees surveyed during summer and winter. Panels represent the 14 sampled plots, arranged by tree-density class: low (<4 trees), medium (4–6 trees) and high (>6 trees per plot). Each colour identifies an individual tree, with summer profiles shown as dashed lines and winter profiles as dotted lines. Tree heights derived from the corresponding TLS point clouds are provided in the panel legends. Horizontal orange and purple lines indicate the plot-specific heights at which the smoothed median F1 profile had declined by 20% relative to its lower-canopy reference value during summer and winter, respectively. Profiles were smoothed before threshold estimation, and a decline was retained only when it persisted across two consecutive height bands. The results show that voxel agreement was generally greatest in the lower portions of trees and declined towards the upper stem and crown, although the magnitude and height of this decline varied among plots, trees and seasons.



936

937 **Figure S8:** Relationship between tree size and the absolute percentage error of TLS-

938 scaled Luma AI estimates for (a) tree height and (b) crown area. Tree height was

939 calculated as the difference between the maximum and minimum z coordinates, while

940 crown area was calculated from the convex hull of the horizontal point-cloud projection.

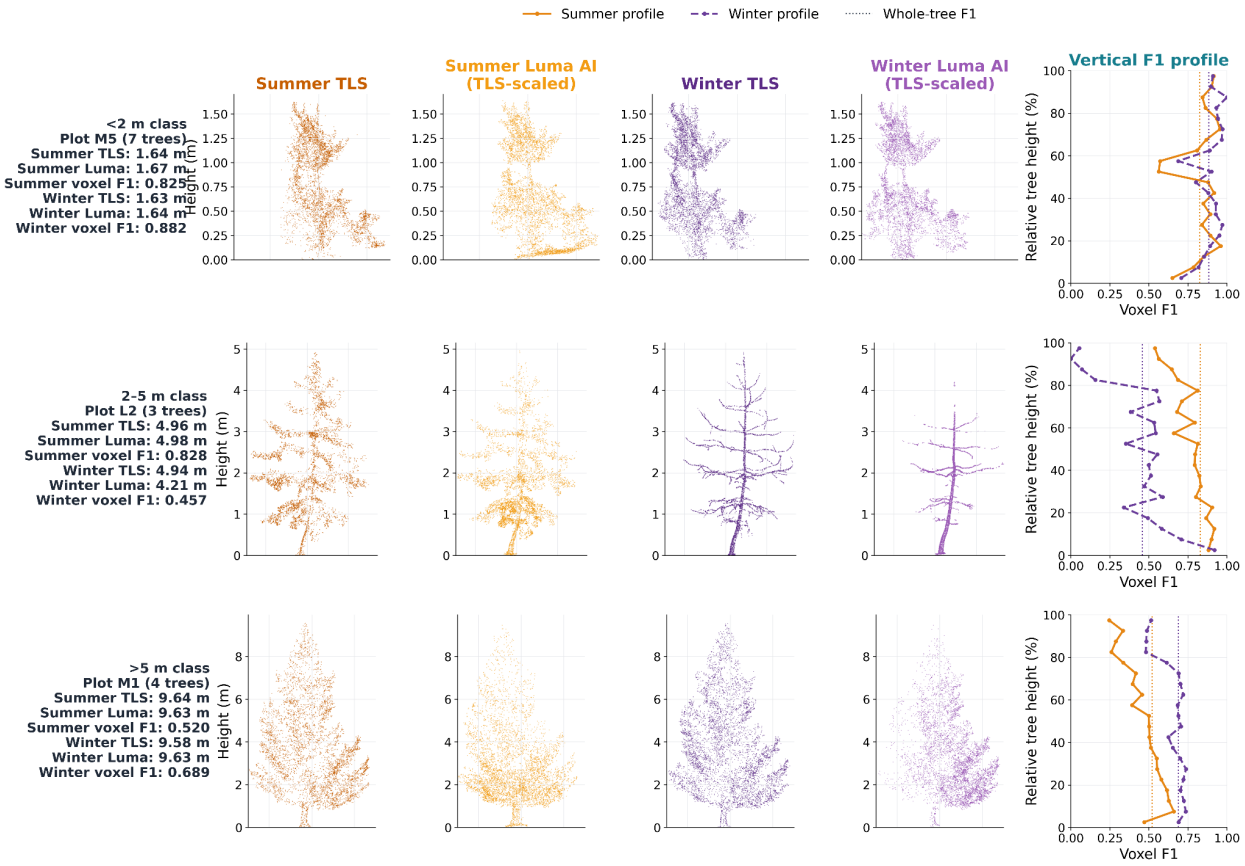
941 Orange and purple points represent summer and winter observations, respectively. Solid

942 lines show least-squares trends for visualisation, while associations were evaluated using

943 Spearman's rank correlation. Absolute percentage error was not significantly associated

944 with tree height or crown area in either season (all $p \geq 0.465$), indicating that proportional

945 structural error did not systematically increase with tree size.



946

947 **Figure S9:** Summer and winter reconstruction performance for selected trees
948 representing three TLS-derived height classes: <2 m, 2–5 m and >5 m. Trees were
949 selected according to the highest whole-tree voxel F1 observed in either season within
950 each height class, after which results from both seasons were displayed for the same
951 tree. Columns show the summer TLS and TLS-scaled Luma AI point clouds, winter TLS
952 and TLS-scaled Luma AI point clouds, and the corresponding vertical F1 profiles. Orange
953 and purple lines represent summer and winter, respectively, while dotted vertical lines
954 indicate whole-tree F1. The tree below 2 m retained consistently high agreement during
955 both seasons. The 2–5 m tree performed strongly during summer but substantially less
956 well during winter, while the tree above 5 m showed moderate agreement, with better

performance during winter than summer. These examples illustrate that reconstruction quality was influenced by season and individual-tree conditions in addition to tree height.

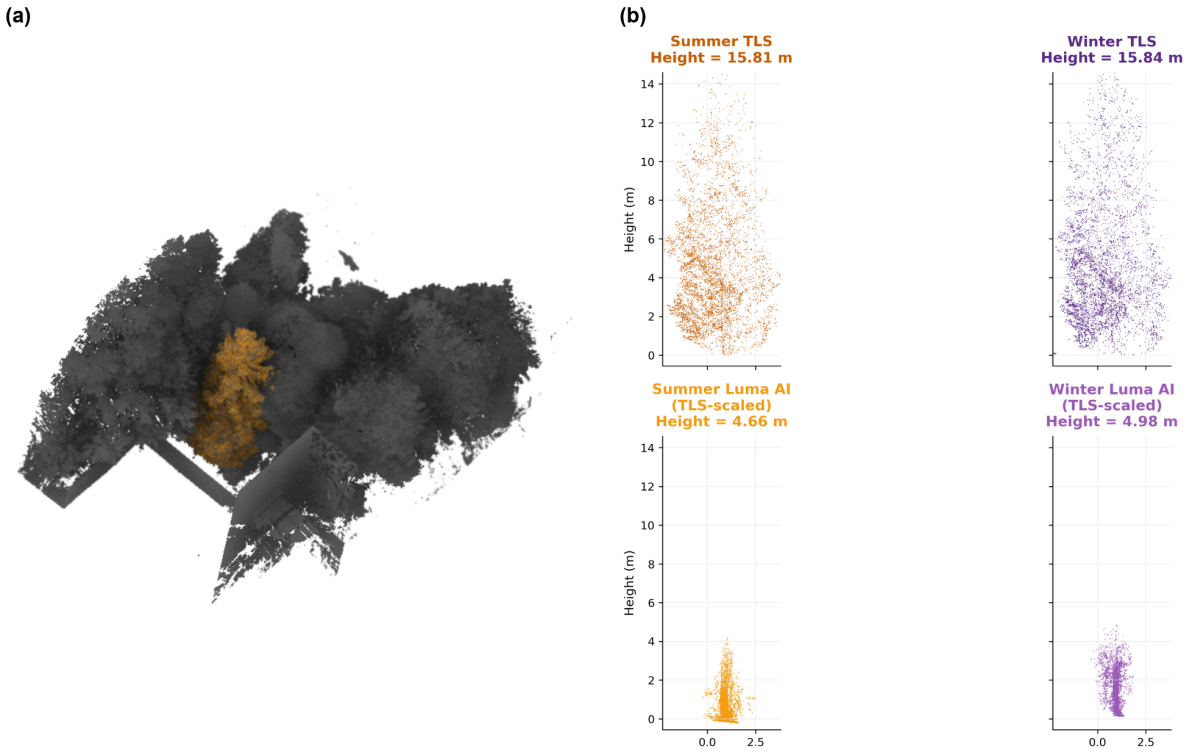


Figure S10: Example of incomplete tree reconstruction caused by the combined effects of surrounding vegetation and restricted physical access. (a) Summer TLS point cloud showing the focal pine in orange and surrounding vegetation in grey. The tree was embedded within neighbouring vegetation and could not be approached from all directions because access around it was restricted. (b) Seasonal comparison of the TLS reference and TLS-scaled Luma AI reconstructions. The TLS-derived tree height was 15.81 m in summer and 15.84 m in winter, whereas Luma AI reconstructed only the lower portion of the tree, producing heights of 4.66 and 4.98 m, respectively. Although the number of trees and total crown area characterised vegetation density, these competition

indicators did not represent physical barriers or the accessibility of suitable camera viewpoints. This example illustrates how vegetation occlusion and restricted access can jointly limit image overlap and reconstruction completeness without being fully captured by the plot-level competition metrics used in this study. Orange and purple represent summer and winter, respectively.